Highlight Review

Synthesis and Structure-specific Functions of Patchy Nanoparticles

Toshiharu Teranishi,* Masaki Saruyama, and Masayuki Kanehara

(Received December 25, 2008; CL-088014)

Abstract

Anisotropically phase-segregated nanoparticles, so-called patchy nanoparticles, are promising materials, because the close coupling of different components on the nanoscale may significantly improve application performance or even create new properties. We demonstrate that the seed-mediated growth method is quite effective in synthesizing various kinds of patchy nanoparticles consisting of a combination of metals, metal sulfides, and metal oxides.

♦ Introduction

Chemically synthesized inorganic nanoparticles (NPs) are composed of inorganic cores surrounded by organic surfactants. To elucidate the chemical and physical properties of the inorganic NPs consisting of one chemical species, precise control of size, shape, and crystal structure is indispensable.[1] When the inorganic cores include more than two chemical species with a combination of metals, metal chalcogenides, and metal oxides, the composition and distribution of each species provide additional parameters that should be controlled.[2] Focusing on the distribution of the two chemical species in a single NP, we can have three kinds of structures dependent on the distribution manner, that is, the chemically disordered alloy, layered core/shell, and anisotropic phase-segregation structures, as shown in Figure 1. In general, the NPs with two chemical species obtained by conventional chemical syntheses have either an alloy or core–shell structure, both of which are isotropic in the light of phase segregation. On the other hand, anisotropically phase-segregated NPs, so-called patchy NPs, have recently become accessible and received much attention. The close coupling of different components on the nanoscale may significantly improve the application performance or even create new properties.[3–29] Figure 2 shows the representative noble properties peculiar to the structure of patchy NPs, as described below.

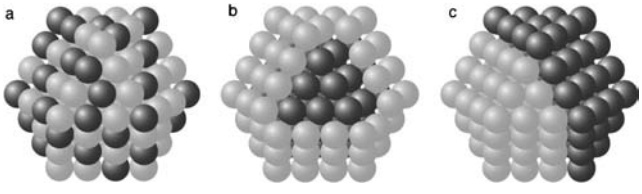

Figure 1. Three kinds of structures of NPs consisting of two chemical species: (a) alloy, (b) core/shell, (c) anisotropic phase-segregation structures.

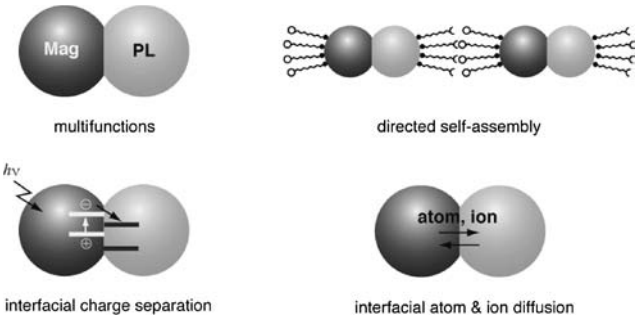

Figure 2. Structure-specific functions of patchy NPs.

(i) Multifunctions, such as a combination of magnetic and photoluminescent NPs.

(ii) Directed self-assembly, achieved by modifying different functional ligands on each surface.

(iii) Highly efficient charge separation at the hetero-interface in a single NP.

(iv) Creation of innovative materials resulting from atom and ion diffusion at the heterointerface.

Table 1 summarizes the various patchy NPs reported so far, most of which deal with a combination of two distinct chemical species. When synthesizing the biphasic patchy NPs, we can employ seed-mediated growth methods and heat-induced phase segregation by making use of the large interface energy between the two chemical species (Figures 3a and 3b). In the case that the two distinct precursors are simultaneously reacted to produce biphasic patchy NPs, the reaction mechanism usually follows a seed-mediated growth reaction; that is, the selective nucleation of one chemical species is followed by growth of the second one, which emerges by developing an interface of graded composition.[7,8] To obtain further complex patchy structures, there are two representative formation mechanisms, as shown in Figures 3c and 3d. Here, we review our recent results to selectively synthesize metal sulfide/metal sulfide and metal/metal oxide patchy NPs, based on the seed-mediated growth method.

♦ Bi-phasic Metal Sulfide Patchy NPs

Many efforts have been made toward the synthesis of metal chalcogenide patchy NPs for application to achieve efficient charge separation.[25,26] However, the combination of metal sulfides, which are easy to synthesize and exhibit absorption and

Prof. Toshiharu Teranishi, Mr. Masaki Saruyama, Dr. Masayuki Kanehara*
Department of Chemistry, Graduate School of Pure and Applied Sciences, University of Tsukuba, 1-1-1 Tennodai, Tsukuba 305-8571
E-mail: teranisi@chem.tsukuba.ac.jp

Table 1. Representative patchy NPs reported so far

Material	Shape	Path[a]	Ref.
PdS_x/Co_9S_8	acorn	a	7, 36
Cu_2S/In_2S_3	acorn, bottle, larva	a	8
CdSe/Au	dumbbell, bell-tongue	a	9
Au/Fe_3O_4	dumbbell	a	10, 39
FePt/Iron oxide	snowman	a	11
$FePt/CoFe_2O_4$	brick	a	12
(FePt, Au, Fe_3O_4)/Ag	snowman	a	13
$CoPt_3/Au$	snowman	a	14
FePt/Au	snowman	a	15
Co/Au	rod	a	16
FePt/CdS	snowman	b	17
γ-Fe_2O_3/sulfide	snowman	b	18
Pd/γ-Fe_2O_3	dumbbell, flower	c	19
Au/Fe_3O_4	flower	c	20
CdSe/Au	rod, tetrapod	c	21
Pbs/Au	tetrapod	c	22
CdS/(Pt, PtNi, PtCo)	rod	c	23
CdSe/(CdS, CdTe)	rod, branched rod	c	24
CdSe/CdS	rod, tetrapod	c	25
CdSe/CdTe	barbell	c	26
Au/Ag	rod	c	27
PdS_x/Co_9S_8	peanut	d	28
(PdS_x, Pd_xCd_yS)/CdS	flower, dumbbell	c, d	29

[a]Formation path shown in Figure 3.

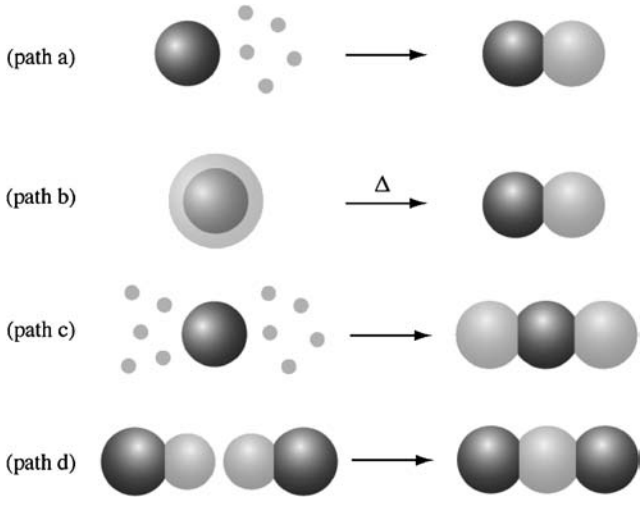

Figure 3. Schematic illustrations of possible mechanisms to form patchy NPs: (path a) selective nucleation on a starting seed, (path b) heat-induced phase segregation, (path c) several nucleations on a starting seed, (path d) fusion of two reactive phases from two distinct biphasic patchy NPs.

emission properties in a wide wavelength region, is still rare,[8] and, therefore, the development of a facile synthesis of metal sulfide patchy NPs is very important.

Through the systematic syntheses of NPs composed of both 3d-transition metals and noble metals for magnetic studies,[30–32] we found that the anisotropically phase-segregated acorn-shaped PdS_x/Co_9S_8 NPs (PdCo sulfide nanoacorns) are spontaneously formed, in which one phase is made up of cobalt sulfide and another of palladium sulfide.[7] The PdCo sulfide nanoacorns were synthesized by the reaction of $Co(acac)_2 \cdot 2H_2O$ and $Pd(acac)_2$ in di-*n*-octyl ether in the presence of 1-octadecanethiol ($C_{18}SH$). Figure 4a shows a low-magnification TEM image of the resulting $C_{18}S$-protected nanoacorns. The acorn-shaped particles made up of both bright and dark phases having an average size of ca. 14 nm (length) × 10 nm (width) and a Co/Pd atomic ratio of 40/60 were predominantly observed. The nanospot energy-dispersive X-ray (EDX), the detailed high-resolution transmission electron microscopy (HRTEM, Figure 4b), and the powder X-ray diffraction (XRD, Figure 4c) measurements revealed that the PdCo sulfide nanoacorns are made up of crystalline Co_9S_8 and amorphous PdS_x phases with an interfacial lattice plane of a Co_9S_8 phase as the (001) plane (Figure 4d).

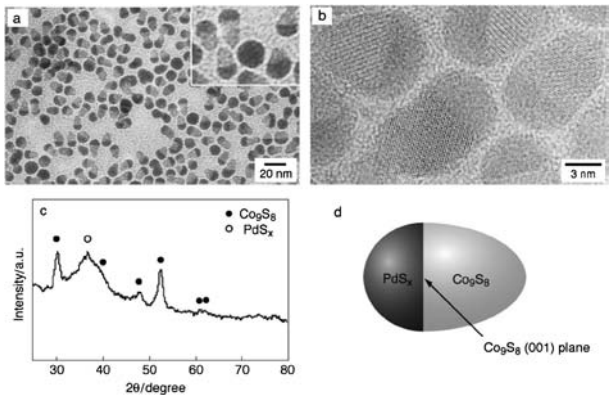

Figure 4. (a) TEM image, (b) high-resolution TEM image, (c) XRD pattern, and (d) schematic illustration of PdCo sulfide nanoacorns (inset in (a), enlarged TEM image) (from ref 7, T. Teranishi et al., *J. Am. Chem. Soc.* **2004**, *126*, 9915, with permission from the American Chemical Society @ 2004).

The formation mechanism of the PdCo sulfide nanoacorns was monitored spectroscopically and microscopically and clarified as follows: (i) the reduction of Pd^{II} ions with $C_{18}SH$ to yield very small $Pd_n(SC_{18})_m$ NPs;[33] (ii) the formation of amorphous PdS_x NPs by the spontaneous cleavage of the C–S bond of $C_{18}S$ at the surface of the metallic palladium to liberate the sulfur atoms,[34,35] which transform the Pd NPs into the palladium sulfide NPs; (iii) the anisotropic growth of the Co_9S_8 phases in the [00$\bar{1}$] direction by the supply of S^{2-} ions from PdS_x NPs to form the PdCo sulfide nanoacorns. The overall formation mechanism of the PdCo sulfide nanoacorns is schematically illustrated in Figure 5, where the important point is the first nucleation of the PdS_x NPs followed by the anisotropic growth of the Co_9S_8 phases (path a in Figure 3). This concept was exploited to form biphasic CuIn sulfide patchy NPs from the coreaction of the respective precursors under suitable conditions.[8] Since a single patchy NP has chemically distinct plural surfaces, it is difficult to completely passivate the surface with one kind of protective ligand in order to prevent the formation of precipitates. The use of several kinds of protective ligands is expected to make the patchy NPs stable in solution.[36]

♦ *Triphasic Metal Sulfide Patchy NPs*

On the basis of our proposed mechanism for the formation of PdCo sulfide nanoacorns, in which the Co_9S_8 phases anisotropically grow from the preformed PdS_x NPs, the PdS_x NPs

Published on the web (Advance View) February 14, 2009; doi:10.1246/cl.2009.194

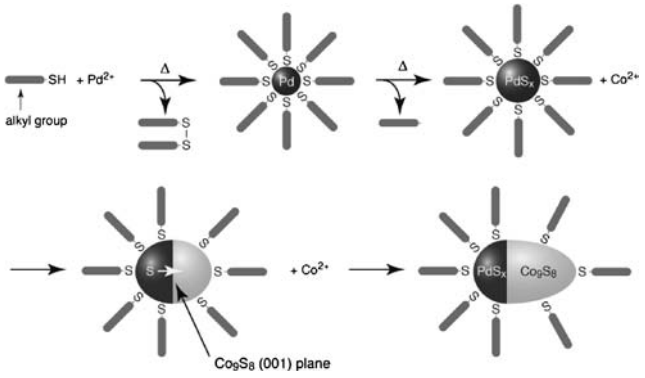

Figure 5. Schematic illustration of the speculated formation mechanism of the PdCo sulfide nanoacorns (from ref 7, T. Teranishi et al., *J. Am. Chem. Soc.* **2004**, *126*, 9915, with permission from the American Chemical Society @ 2004).

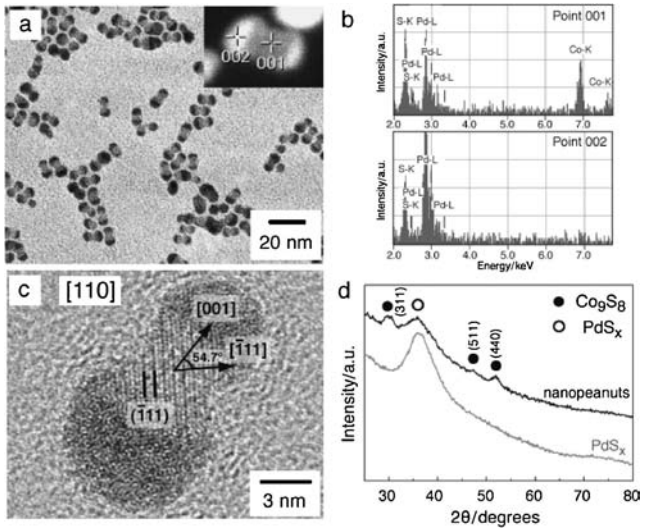

Figure 6. (a) TEM image of PdCoPd sulfide nanopeanuts (inset, STEM-HAADF image), (b) EDX spectra of the bright and dark regions of nanopeanuts marked by crosses in (a), (c) High-resolution TEM image of a single nanopeanut when observed in the [110] direction, and (d) XRD patterns of PdS_x and PdCoPd sulfide nanopeanuts (from ref 28, T. Teranishi et al., *Angew. Chem., Int. Ed.* **2007**, *46*, 1713, with permission from Wiley-VCH @ 2007).

are the key material for the formation of heterostructures. Accordingly, the PdS_x seed-mediated synthesis of anisotropically phase-segregated NPs was carried out.[28] The relatively monodisperse 5.6 ± 1.0 nm PdS_x NPs were synthesized as seeds by making use of the spontaneous cleavage of the C–S bonds of $C_{18}S$ on the surfaces of the Pd NPs.[34,35] The Co_9S_8 phases were anisotropically grown on the surface of the purified PdS_x seeds by reacting the PdS_x seeds with $Co(acac)_2$ and $C_{18}SH$ in di-*n*-octyl ether at 230 °C for 40 min under nitrogen. Figure 6a shows a low-magnification TEM image of the resulting NPs. The peanut-shaped NPs (nanopeanuts) made up of bright phases with dark phases at either end, and having an average size of ca. 10 nm (length) × 5 nm (width), were predominantly observed together with a minor fragment of nanoacorns, where the size of the PdS_x NPs was preserved. The compositional variation along the length of the nanopeanuts is apparent in the dark field scanning transmission electron microscopy (STEM) image taken using a high angle annular dark field (HAADF) detector (inset in Figure 6a). This Z-contrast image shows the brighter Pd species isolated in the peanut ends and the darker Co species in the peanut core. Figure 6b presents nanospot EDX spectra of the dark and bright phases of a nanopeanut, as marked by crosses in the STEM-HAADF image, confirming that the cobalt and palladium atoms were mainly located in the dark and bright phases in the STEM-HAADF image, respectively. The crystal structural investigation of these nanopeanuts, including HRTEM (Figure 6c) and XRD (Figure 6d) measurements, reveals that the nanopeanuts have an amorphous PdS_x/crystalline Co_9S_8/amorphous PdS_x (PdCoPd sulfide) heterostructure with two interfacial lattice planes of Co_9S_8 phases as the (001) plane, which is observed for the PdCo sulfide nanoacorns.

It is expected from the shape of the nanopeanuts that they are formed by fusing together two PdCo sulfide nanoacorns. Actually, once the spherical PdCo sulfide nanoacorns are formed, the less-passivated Co_9S_8 phases of the nanoacorns are easily fused at their further growth stage in the $[00\bar{1}]$ direction to yield PdCoPd sulfide nanopeanuts. In the fusion process, two PdCo sulfide nanoacorns appear to fuse together by facing each other with their Co_9S_8 phases aligned in the same crystallographic orientation, following path d in Figure 3. Here, we consider that the key factor determining whether the fusion of the two Co_9S_8 phases proceeds or not is the amount of passivating agent, $C_{18}SH$, added to grow the Co_9S_8 phases. It was reasonably concluded from additional experiments that the less-passivated PdCo sulfide nanoacorns ($C_{18}SH/Co(acac)_2 \leq 2$) easily form nanopeanuts via the fusion of two Co_9S_8 phases to reduce interface free energies of the less-passivated Co_9S_8 phases, whereas the fusion of the nanoacorns synthesized at $C_{18}SH/Co(acac)_2 \geq 3$ is suppressed owing to the sufficient passivation of the Co_9S_8 surfaces by thiols, as shown in Figure 7.

Extension of the kinds of metal sulfide seeds is requisite for the designed synthesis of various metal sulfide patchy NPs. Recently, we have demonstrated that CdPd sulfide patchy NPs can be selectively synthesized from various seed-mediated growth methods.[29] In the PdS_x seed-mediated growth, the crystal structural transformation from amorphous PdS_x to crystalline Pd_xCd_yS phases by the cation exchange of Cd^{2+} with Pd^{2+} (cf., the cation exchange of smaller Co^{2+} ions with Pd^{2+} does not occur) and the subsequent diffusion of S^{2-} take place to form the flower-shaped Pd_xCd_yS/CdS patchy NPs, as shown in Figure 8a, following path c in Figure 3. The Pd_xCd_yS/CdS interfacial lattice planes of the CdS phases correspond to zinc blende (zb)-CdS (002), (111) and wurtzite (w)-CdS (100). An ionic crystal containing the elements Cd, Pd, and S was not identified in the *Powder Diffraction File* (JCPDS-ICDD). From the detailed HRTEM and fast Fourier transformation (FFT) investiga-

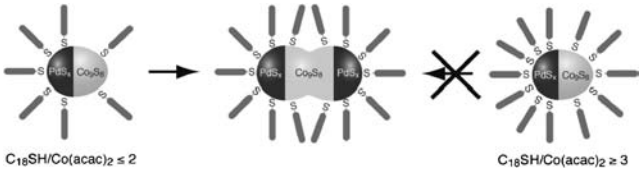

Figure 7. Schematic illustration of the speculated formation mechanism of the PdCoPd sulfide nanopeanuts.

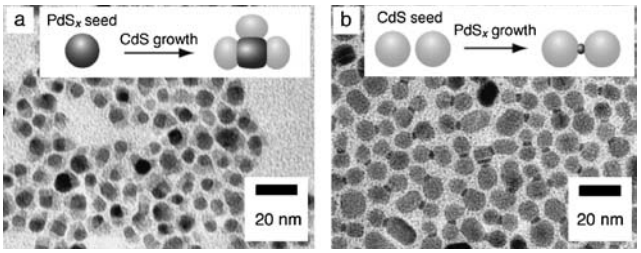

Figure 8. TEM images of (a) flower-shaped Pd_xCd_yS/CdS and (b) dumbbell-shaped $CdS/PdS_x/CdS$ patchy NPs. Insets show the schematic illustrations of the formation mechanism.

tions, we assume that the Pd_xCd_yS phase belongs to a cubic crystal system with a lattice constant of 7.92 Å. Sophisticated dumbbell-shaped w-CdS/PdS_x/w-CdS patchy NPs with the interfacial lattice planes of the w-CdS phase as (100) planes, were formed by bridging CdS seeds with PdS_x phases (Figure 8b) using the CdS seed-mediated growth reaction, following path d in Figure 3. Contrary to the flower-shaped Pd_xCd_yS/CdS patchy NPs, the Pd-rich phases were *amorphous* PdS_x, because the Cd^{2+} ions of the CdS seeds could not diffuse into the newly grown PdS_x phases. The dumbbell-shaped w-CdS/PdS_x/w-CdS patchy NPs were found to be generated by fusing together two PdS_x phases of w-CdS–PdS_x dimers, as observed in the formation of peanut-shaped $PdS_x/Co_9S_8/PdS_x$ NPs. By utilizing this formation mechanism, the self-assembly of CdS nanorods ($6 \times 16\,nm^2$) successfully proceeded via the linkage of CdS nanorods with PdS_x phases. These results confirm that various metal sulfides can be considered as candidate building blocks for creating desirable functional patchy NPs. The partial cation exchange of metal sulfide nanostructures was revealed to be useful to obtain the complex metal sulfide patchy structures like the CdS/Ag_2S nanorods reported by Alivisatos and co-workers.[37,38]

♦ *Metal/Oxide Patchy NPs*

The patchy NPs formed with a combination of metal and metal oxide were also investigated mainly with the aim of achieving bifunctionality, such as optical and magnetic functions. The most useful method to obtain metal/oxide patchy NPs is the metal NP seed-mediated growth synthesis, in which the crystalline metal oxide phases are anisotropically grown on the crystalline metal NPs in a heteroepitaxial fashion driven by the lattice-mismatch strains. Sun and co-workers succeeded in synthesizing dumbbell-shaped Au/Fe_3O_4 patchy NPs by refluxing Au NPs with $Fe(CO)_5$ in 1-octadecene in the presence of oleic acid and oleylamine, followed by room-temperature oxidation under air.[10] These Au/Fe_3O_4 patchy NPs were used as dual-functional probes by modifying the NPs with different functional ligands on each surface.[39]

Recently, we have successfully synthesized Pd/γ-Fe_2O_3 patchy NPs, which are interesting in the light of bifunctionality including such properties as catalysis and magnetism. However, what we focused on is the structural transformation of the Pd/γ-Fe_2O_3 patchy NPs into exchange-coupled face-centered tetragonal (fct)-FePd/α-Fe nanocomposite magnets via interfacial atom diffusion of Pd/γ-Fe_2O_3 patchy NPs, as shown in Figure 9a. Exchange-coupled nanocomposite magnets consisting of magnetically hard and soft phases are of great importance for advanced permanent magnetic applications owing to their large energy

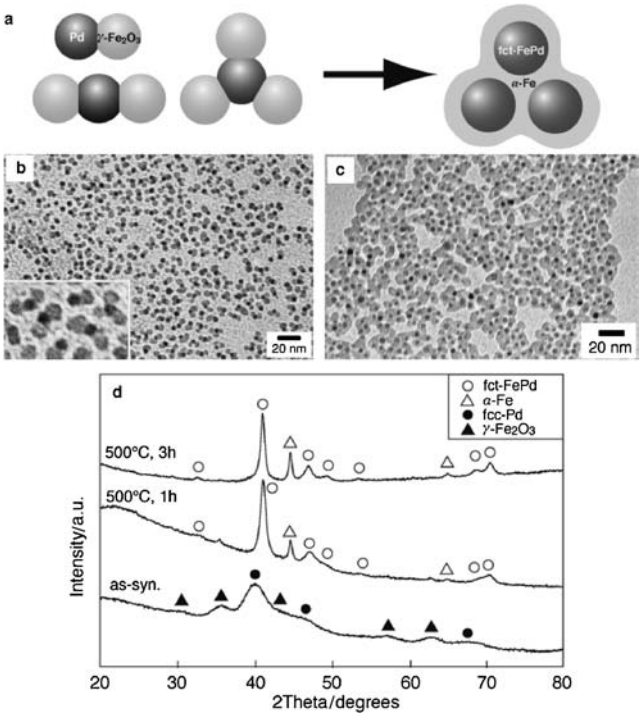

Figure 9. (a) Schematic illustration of the conversion of Pd/γ-Fe_2O_3 NPs into exchange-coupled fct-FePd/α-Fe nanocomposite magnets via the interfacial atom diffusion. (b, c) TEM images of Pd/γ-Fe_2O_3 nanoparticles (b) as-synthesized and (c) after annealing under $Ar + 4\%$ H_2 at 500 °C for 1 h. (d) XRD patterns of as-synthesized and annealed NPs (from ref 19, T. Teranishi et al., *J. Am. Chem. Soc.* **2008**, *130*, 4210, with permission from the American Chemical Society @ 2008).

product compared with conventional single-phase magnets.[40] Control of the hard and soft phases at the nanometer scale is very significant for achieving efficient exchange coupling. Solid-state reactions of assemblies consisting of two distinct NPs are one approach in solving the above problem,[41,42] although the precise control of both phases at the nanometer scale is still a challenging subject. The fct-FePd NPs were chosen as a magnetically hard phase because the face-centered cubic (fcc)-Pd phase can only be converted to fct-FePd phase even in the presence of excess Fe.

Monodisperse 4.9 ± 0.3 nm trioctylphosphine-protected polycrystalline Pd (TOP–Pd) NPs were synthesized[43] and used as seeds. The Pd/γ-Fe_2O_3 patchy NPs were synthesized by the Pd seed-mediated growth synthesis. The 4.9 nm TOP–Pd NPs (Pd = 0.17 mmol) were dissolved in 1-octanol (20 mL), to which $Fe(acac)_3$ (0.43 mmol), oleylamine (6.8 mmol), and oleic acid (6.8 mmol) were added. After stirring the N_2-bubbled solution at 180 °C for 1 h, the heat source was removed to allow the black solution to cool to room temperature. The resulting NPs were purified with 1-hexane/ethanol (1/2, v/v) mixed solvent. Figure 9b shows the TEM image of the resulting NPs. The NPs made up of dark Pd phases with 1–3 bright phases anisotropically grown at every single Pd NP surface (following path c in Figure 3) were predominantly observed, where the size of the Pd NPs was preserved. It was clarified from the HRTEM, XRD, and XPS analyses that the bright phases were composed of γ-Fe_2O_3. The interfacial lattice planes of the two distinct

phases could be the combination of those with the smallest lattice mismatch, but this remains unclear at present. The Fe/Pd molar ratio was estimated to be 73/27 from X-ray fluorescence analysis, which is roughly consistent with the Fe/Pd molar ratio for the feeding precursors and is large enough to convert the Pd/γ-Fe_2O_3 NPs into fct-FePd/α-Fe nanocomposite magnets.

To convert the Pd/γ-Fe_2O_3 NPs into exchange-coupled fct-FePd/α-Fe nanocomposite magnets, the Pd/γ-Fe_2O_3 NPs were annealed under a flow of Ar + 4% H_2 at 500 °C. Figure 9c shows the TEM image of the resulting NPs annealed for 1 h. Patchy NPs were not observed, and the dark phases were incorporated in the bright phase matrix. It was revealed from the XRD (Figure 9d) and HRTEM analyses that the γ-Fe_2O_3 phases were completely converted into body-centered cubic (bcc) α-Fe, while the fcc-Pd was converted into fct-FePd. The long-range-order parameter of fct-FePd for the sample annealed for 3 h was estimated to be 0.25 from the XRD results. It should be noted that the size of the fct-FePd phases (4.9 ± 0.4 nm) is quite similar to that of the fcc-Pd phases. Longer annealing time contributed to an increase in the ordering degree of the fct structure of the FePd phases together with a slight expansion of the phase volume (6.0 ± 1.0 nm). These results lead us to the following conclusion. First the annealing of the Pd/γ-Fe_2O_3 NPs under Ar + 4% H_2 reduces the γ-Fe_2O_3 to bcc α-Fe, which is followed by coalescence to form the α-Fe matrix owing to desorption of the organic ligands around each particle. At the same time, interdiffusion between α-Fe and Pd creates fct-FePd phases in the rich Fe condition, following the phase diagram of the FePd alloy, as observed in the Pt/γ-Fe_2O_3 system.[44] The fct-FePd phases do not grow significantly because they are incorporated into the α-Fe matrix. Finally, magnetically hard fct-FePd phases surrounded by magnetically soft α-Fe phases are obtained. For comparison, a hexagonal lattice consisting of 3.6 nm Fe_3O_4 NPs and 4.9 nm Pd NPs (Fe/Pd = 84/16 (mol/mol)), where two kinds of NPs randomly occupied the site, was annealed under Ar + 4% H_2 at 500 °C for 1 h, forming quite polydisperse NPs having bcc α-Fe and fct-FePd phases. This result strongly demonstrates that the nanoscale interfaces of the Pd/γ-Fe_2O_3 NPs play an important role in forming nanocomposite magnets with controlled structure at the nanometer scale. In addition, both the (111) lattice plane of the fct-FePd hard phase and the (110) plane of the α-Fe soft phase gradually deform to connect with each other (the lattice mismatch = ca. 7.5%), demonstrating effective exchange coupling.

To ensure an efficient exchange coupling between the soft and hard phases, the magnetic properties were measured for the fct-FePd/α-Fe nanocomposites made by the conversion of Pd/γ-Fe_2O_3 NPs at 500 °C for 3 h using VSM. Figure 10 shows the magnetization curves of the Pd/γ-Fe_2O_3 before and after annealing. The saturation magnetization (M_s), remanent magnetization (M_r), and coercivity (H_c) for the annealed specimen were 114 emu·g^{-1}, 73.4 emu·g^{-1}, and 755 Oe, respectively. The M_s value was between those for α-Fe (217 emu·g^{-1}) and fct-FePd (111 emu·g^{-1}), and the H_c value was smaller than that for bulk fct-FePd, which may result from the low long-range-order parameter of FePd, the unoptimized soft/hard volume ratio (58/42), and the particle size, because the dimension of the soft phase should be smaller than twice the domain wall width of the hard phase to allow effective exchange coupling to occur within a two-phase magnet.[4] However, the characteristic magnetization process such as that of a single-phase hard magnet indicates the existence of an effective exchange coupling between the hard and soft phases in the present specimen.

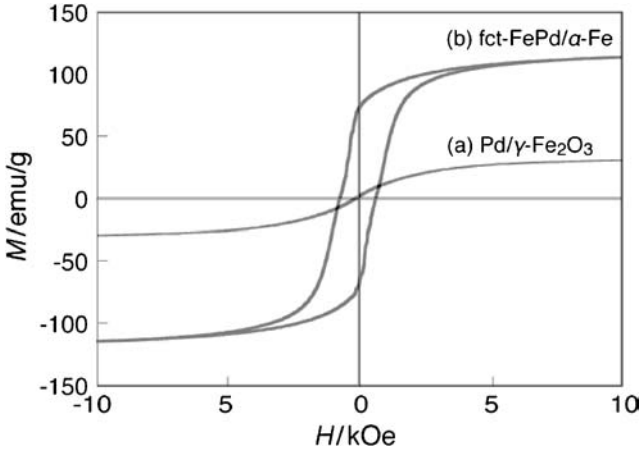

Figure 10. Magnetization curves of Pd/γ-Fe_2O_3 NPs (a) before and (b) after annealing under a flow of Ar + 4% H_2 at 500 °C for 3 h. The measurement was conducted at room temperature with a maximum application field of 10 kOe (from ref 19, T. Teranishi et al., *J. Am. Chem. Soc.* **2008**, *130*, 4210, with permission from the American Chemical Society @ 2008).

♦ Conclusions and Prospects

The seed-mediated growth synthesis and structure-specific functions of various patchy NPs were presented. It was demonstrated that various metals and metal sulfides could be considered as candidate building blocks for creating desirable functional patchy NPs. This would lead to the following prospects for the patchy NPs:

(i) Enrichment of the patchy NP library.

(ii) Programmable assembly of NPs induced by the selective modification of the NP surface by the different ligands.

(iii) Creation of various innovative materials by the hetero-interfacial atom or ion diffusion.

(iv) Realization of heterointerfacial charge separation.

Patchy NPs have a great potential to provide novel functional materials by making use of their structure specificity.

This work was supported by a Grant-in-Aid for Exploratory Research (No. 20655027) and Scientific Research on Priority Area "Strong Photon–Molecule Coupling Fields" (No. 19049007) (T.T.) and a Research Fellowship of JSPS for Young Scientists (M.S.).

References

1 T. Teranishi, in *Encyclopedia of Surface and Colloid Science*, ed. by A. Hubbard, Marcel Dekker, New York, **2002**, pp. 3314–3327.
2 T. Teranishi, N. Toshima, in *Catalysis at Nanoparticle Surfaces*, ed. by A. Wieckowski, E. R. Savinova, C. G. Vayenas, Marcel Dekker, New York, **2002**, pp. 379–407.
3 A. Perro, S. Reculusa, S. Ravaine, E. Bourgeat-Lami, E. Duguet, *J. Mater. Chem.* **2005**, *15*, 3745.
4 P. D. Cozzoli, T. Pellegrino, L. Manna, *Chem. Soc. Rev.* **2006**, *35*, 1195.

5 T. Teranishi, *Small* **2006**, *2*, 596.
6 M. Casavola, R. Buonsanti, G. Caputo, P. D. Cozzoli, *Eur. J. Inorg. Chem.* **2008**, 837.
7 T. Teranishi, Y. Inoue, M. Nakaya, Y. Oumi, T. Sano, *J. Am. Chem. Soc.* **2004**, *126*, 9914.
8 S.-H. Choi, E.-G. Kim, T. Hyeon, *J. Am. Chem. Soc.* **2006**, *128*, 2520.
9 T. Mokari, C. G. Sztrum, A. Salant, E. Rabani, U. Banin, *Nat. Mater.* **2005**, *4*, 855.
10 H. Yu, M. Chen, P. M. Rice, S. X. Wang, R. L. White, S. Sun, *Nano Lett.* **2005**, *5*, 379.
11 A. Figuerola, A. Fiore, R. D. Corato, A. Falqui, C. Giannini, E. Micotti, A. Lascialfari, M. Corti, R. Cingolani, T. Pellegrino, P. D. Cozzoli, L. Manna, *J. Am. Chem. Soc.* **2008**, *130*, 1477.
12 G. S. Chaubey, V. Nandwana, N. Poudyal, C.-B. Rong, J. P. Liu, *Chem. Mater.* **2008**, *20*, 475.
13 H. Gu, Z. Yang, J. Gao, C. K. Chang, B. Xu, *J. Am. Chem. Soc.* **2005**, *127*, 34.
14 T. Pellegrino, A. Fiore, E. Carlino, C. Giannini, P. D. Cozzoli, G. Ciccarella, M. Respaud, L. Palmirotta, R. Cingolani, L. Manna, *J. Am. Chem. Soc.* **2006**, *128*, 6690.
15 J.-S. Choi, Y.-W. Jun, S.-I. Yeon, H. C. Kim, J.-S. Shin, J. Cheon, *J. Am. Chem. Soc.* **2006**, *128*, 15982.
16 F. Wetz, K. Soulantica, A. Falqui, M. Respaud, E. Snoeck, B. Chaudret, *Angew. Chem., Int. Ed.* **2007**, *46*, 7079.
17 H. Gu, R. Zheng, X. Zhang, B. Xu, *J. Am. Chem. Soc.* **2004**, *126*, 5664.
18 K.-W. Kwon, M. Shim, *J. Am. Chem. Soc.* **2005**, *127*, 10269.
19 T. Teranishi, A. Wachi, M. Kanehara, T. Shoji, N. Sakuma, M. Nakaya, *J. Am. Chem. Soc.* **2008**, *130*, 4210.
20 Y. Wei, R. Klajn, A. O. Pinchuk, B. A. Grzybowski, *Small* **2008**, *4*, 1635.
21 T. Mokari, E. Rothenberg, I. Popov, R. Costi, U. Banin, *Science* **2004**, *304*, 1787.
22 J. Yang, H. I. Elim, Q. Zhang, J. Y. Lee, W. Ji, *J. Am. Chem. Soc.* **2008**, *130*, 3294.
23 S. E. Habas, P. Yang, T. Mokari, *J. Am. Chem. Soc.* **2008**, *130*, 3294.
24 D. J. Milliron, S. M. Hughes, Y. Cui, L. Manna, J. Li, L.-W. Wang, A. P. Alivisatos, *Nature* **2004**, *430*, 190.
25 D. V. Talapin, J. H. Nelson, E. V. Shevchenko, S. Aloni, B. Sadtler, A. P. Alivisatos, *Nano Lett.* **2007**, *7*, 2951.
26 J. E. Halpert, V. J. Porter, J. P. Zimmer, M. G. Bawendi, *J. Am. Chem. Soc.* **2006**, *128*, 12590.
27 D. Seo, C. I. Yoo, J. Jung, H. Song, *J. Am. Chem. Soc.* **2008**, *130*, 2940.
28 T. Teranishi, M. Saruyama, M. Nakaya, M. Kanehara, *Angew. Chem., Int. Ed.* **2007**, *46*, 1713.
29 M. Saruyama, M. Kanehara, T. Teranishi, submitted.
30 T. Teranishi, M. Miyake, *Chem. Mater.* **1999**, *11*, 3414.
31 M. Nakaya, Y. Tsuchiya, K. Ito, Y. Oumi, T. Sano, T. Teranishi, *Chem. Lett.* **2004**, *33*, 130.
32 M. Nakaya, M. Kanehara, T. Teranishi, *Langmuir* **2006**, *22*, 3485.
33 Y. Negishi, H. Murayama, T. Tsukuda, *Chem. Phys. Lett.* **2002**, *366*, 561.
34 J. C. Love, D. B. Wolfe, R. Haasch, M. L. Chabinyu, K. E. Paul, G. M. Whitesides, R. G. Nuzzo, *J. Am. Chem. Soc.* **2003**, *125*, 2597.
35 H. Murayama, N. Ichikuni, Y. Negishi, T. Nagata, T. Tsukuda, *Chem. Phys. Lett.* **2003**, *376*, 26.
36 T. Teranishi, Y. Inoue, M. Saruyama, M. Nakaya, M. Kanehara, *Chem. Lett.* **2007**, *36*, 490.
37 R. D. Robinson, B. Sadtler, D. O. Demchenko, C. K. Erdonmez, L.-W. Wang, A. P. Alivisatos, *Science* **2007**, *317*, 355.
38 D. O. Demchenko, R. D. Robinson, B. Sadtler, C. K. Erdonmez, A. P. Alivisatos, L.-W. Wang, *ACS Nano* **2008**, *2*, 627.
39 C. Xu, J. Xie, D. Ho, C. Wang, N. Kohler, E. G. Walsh, J. R. Morgan, Y. E. Chin, S. Sun, *Angew. Chem., Int. Ed.* **2008**, *47*, 173.
40 R. Skomski, J. M. D. Coey, *Phys. Rev. B* **1993**, *48*, 15812.
41 H. Zeng, J. Li, J. P. Liu, Z. L. Wang, S. Sun, *Nature* **2002**, *420*, 395.
42 J. Cheon, J. Park, J. Choi, Y. Jun, S. Kim, M. G. Kim, Y. Kim, Y. J. Kim, *Proc. Natl. Acad. Sci. U.S.A.* **2006**, *103*, 3023.
43 S. Kim, J. Park, Y. Jang, Y. Chung, S. Hwang, T. Hyeon, *Nano Lett.* **2003**, *3*, 1289.
44 X. Teng, H. Yang, *J. Am. Chem. Soc.* **2003**, *125*, 14559.